JOURNAL OF GEOPHYSICAL RESEARCH, VOL. 114, D18120, doi:10.1029/2009JD011733, 2009

Click Here for Full Article

An empirical seasonal prediction model of the east Asian summer monsoon using ENSO and NAO

Zhiwei Wu,[1,2] Bin Wang,[2] Jianping Li,[1] and Fei-Fei Jin[2]

Received 8 January 2009; revised 2 July 2009; accepted 13 July 2009; published 29 September 2009.

[1] How to predict the year-to-year variation of the east Asian summer monsoon (EASM) is one of the most challenging and important tasks in climate prediction. It has been recognized that the EASM variations are intimately but not exclusively linked to the development and decay of El Niño or La Niña. Here we present observed evidence and numerical experiment results to show that anomalous North Atlantic Oscillation (NAO) in spring (April–May) can induce a tripole sea surface temperature pattern in the North Atlantic that persists into ensuing summer and excite downstream development of subpolar teleconnections across the northern Eurasia, which raises (or lowers) the pressure over the Ural Mountain and the Okhotsk Sea. The latter strengthens (or weakens) the east Asian subtropical front (Meiyu-Baiu-Changma), leading to a strong (or weak) EASM. An empirical model is established to predict the EASM strength by combination of the El Niño–Southern Oscillation (ENSO) and spring NAO. Hindcast is performed for the 1979–2006 period, which shows a hindcast prediction skill that is comparable to the 14 state-of-the-art multimodel ensemble hindcast. Since all these predictors can be readily monitored in real time, this empirical model provides a real time forecast tool.

Citation: Wu, Z., B. Wang, J. Li, and F.-F. Jin (2009), An empirical seasonal prediction model of the east Asian summer monsoon using ENSO and NAO, *J. Geophys. Res.*, *114*, D18120, doi:10.1029/2009JD011733.

1. Introduction

[2] The poor simulation of the Indian monsoon was noted by many previous studies [e.g., *Sperber and Palmer*, 1996; *Gadgil and Sajani*, 1998; *Wang et al.*, 2004], yet the east Asian summer monsoon (EASM) has only recently been revealed as a major challenge in numerical simulation [*Kang et al.*, 2002; *Wang et al.*, 2004] and seasonal prediction [e.g., *Chang*, 2004; *Wang et al.*, 2005; *Wu and Li*, 2008]. The multimodel ensemble (MME) is generally better than any single model prediction [*Doblas-Reyes et al.*, 2000; *Palmer et al.*, 2000; *Krishnamurti et al.*, 1999], providing an effective way to aggregate and synthesize multimodel forecasts [*Wang et al.*, 2008a]. However, examination of the ensemble of five state-of-the-art atmospheric general circulation models' (AGCMs) 20-year (1979–1998) hindcast experiment indicates that the ensemble skill of these models remains very low in forecasting the EASM [*Wang et al.*, 2005]. Therefore, determination of the predictability of the EASM and identification of the sources of predictability are of central importance to seasonal prediction of the EASM and associated uncertainties [*Wang et al.*, 2008b].

[3] It has been generally recognized that the EASM experiences strong interannual variations associated with the El Niño–Southern Oscillation (ENSO) [e.g., *Fu and Teng*, 1988; *Weng et al.*, 1999, *Wang et al.*, 2000, 2008c; *Chang et al.*, 2000a, 2000b; *Yang and Lau*, 2006]. In the last 30 years, the dominant empirical orthogonal function mode indicates that an enhanced east Asian subtropical front and abundant Meiyu occur during the summer when El Niño decays [*Wang et al.*, 2008c]. Why is there a "delayed" response of the EASM to ENSO in the ensuing summer when sea surface temperature (SST) anomalies disappear in the tropical eastern central Pacific? *Wang et al.* [2000] pointed out that the interaction between the off-equatorial moist atmospheric Rossby waves and the underlying SST anomalies in the western Pacific warm pool region can "prolong" the impacts of ENSO from its mature phase to decaying phase and causes a "delayed" response of the EASM to ENSO. Nevertheless, since the EASM has complex spatial and temporal structures that encompass tropics, subtropics, and midlatitudes, its variability is influenced not only by the variations originated from the tropics (i.e., ENSO) [e.g., *Chen and Chang*, 1980; *Huang and Lu*, 1989; *Wu et al.*, 2000; *Ding*, 2004; *Ninomiya*, 2004; *Wu et al.*, 2006], but also by those from the midlatitudes to high latitudes [e.g., *Enomoto et al.*, 2003; *Wu et al.*, 2006; *He et al.*, 2006; *Ding and Wang*, 2007].

[4] North Atlantic Oscillation (NAO) is a large-scale seesaw in atmospheric mass between the subtropical high and the polar low [e.g., *Walker and Bliss*, 1932; *Bjerknes*, 1964; *van Loon and Rogers*, 1978; *Wallace and Gutzler*, 1981; *Barnston and Livezey*, 1987; *Li and Wang*, 2003]. *Trenberth et al.* [2005] suggested that the Northern Hemisphere annual mode and associated NAO is the third most

[1]State Key Laboratory of Numerical Modeling for Atmospheric Sciences and Geophysical Fluid Dynamics, Institute of Atmospheric Physics, Chinese Academy of Sciences, Beijing, China.
[2]Department of Meteorology and IPRC, University of Hawai'i at Mānoa, Honolulu, Hawaii, USA.

Copyright 2009 by the American Geophysical Union.
0148-0227/09/2009JD011733$09.00

important pattern of global atmospheric mass interannual variability. A few studies have already noticed that NAO may affect Asian climate. *Chang et al.* [2001] suggested that the weakening Indian monsoon rainfall–ENSO relationship since 1970s is most likely due to strengthened NAO on the interdecadal time scale. *Watanabe* [2004] found that NAO signals are relatively confined to the Euro-Atlantic sector in December while it extends toward east Asia and the North Pacific in February on the interannual time scale.

[5] Although NAO signals associated with the North Atlantic storm track tend to be weakened from spring to summer [*Lau and Nath*, 1991; *Jin et al.*, 2006a, 2006b], it is still not clear whether spring (April–May) NAO can affect variations of the EASM or not. If so, how does it work and to what extent does it contribute to the seasonal prediction of the EASM? In this paper we attempt to answer these questions.

[6] In section 2, we describe the data sets and the numerical model used in this study. The distinctive rainfall and circulation structures of a strong EASM is briefly described in section 3 as background information. The statistical relationship among spring NAO, North Atlantic SSTs, and the EASM is manifested in section 4. Section 5 investigates the possible physical mechanism on how spring NAO affects the EASM variations. In section 6, an empirical model is established to forecast the strength of the EASM based on ENSO and spring NAO, and a hindcast is performed for the 1979–2006 period. In section 7, the main conclusions are summarized, and some outstanding issues are discussed.

2. Data and Model

[7] The main data sets employed in this study include (1) monthly precipitation data from the global land precipitation reconstruction over land (PREC/L) data for the 1979–2006 period gridded at 1.0° × 1.0° resolution [*Chen et al.*, 2002]; (2) monthly circulation data, gridded at 2.5° × 2.5° resolution, taken from the National Centers for Environmental Prediction–Department of Energy reanalysis [*Kanamitsu et al.*, 2002]; and (3) the Niño3.4 SST index calculated from the improved Extended Reconstructed SST Version 2 (ERSST V2) [*Smith and Reynolds*, 2004]. In this study, summer (June, July, and August (JJA)) mean anomalies are defined by the deviation of JJA mean from the long-term (1979–2006) mean climatology, and spring refers to April–May.

[8] All the numerical experiments presented in this paper are based on a dry spectral primitive equation model developed by *Hoskins and Simmons* [1975]. The version used here differs from the original in some details [*Simmons and Burridge*, 1981; *Roads*, 1987; *Lin and Derome*, 1996; *Marshall and Molteni*, 1993; *Hall*, 2000]. The resolution used here is triangular 31, with 10 equally spaced sigma levels. An important feature of this model is that it uses a time-averaged forcing calculated empirically from observed daily data. By computing the dynamical terms of the model, together with a linear damping, with daily global analyses and averaging in time, the residual term for each time tendency equation is obtained as the forcing. This forcing, thus, includes all processes that are not resolved by the model's dynamics such as diabatic heating (including latent heat release related to the transient eddies) and the deviation of dissipative processes from linear damping. The model has no orography, so the forcing also mimics the time mean orographic forcing. Because of its simplicity in physics, it is referred to as a "simple general circulation model" (SGCM). The advantage of this SGCM model is that dynamical mechanisms are more easily isolated, and since the model used is computationally cheap, many experiments can be performed. The limitation of this approach is that the physical parameterizations present in general circulation models are replaced by empirically derived terms, so some potentially important physical feedback mechanisms may be absent from our analysis. As shown by *Hall* [2000], this model is able to reproduce remarkably realistic stationary planetary waves and the broad climatological characteristics of the transients are in general agreement with observations.

3. Structure of Rainfall and Circulations Associated With a Strong EASM

[9] The EASM is a distinctive component of the Asian climate system [*Zhu*, 1934; *Tu and Huang*, 1944; *Chen and Chang*, 1980; *Tao and Chen*, 1987; *Lau et al.*, 1988; *Ding*, 1992; *Wang et al.*, 2001; *Li and Zeng*, 2002; *Wang and Li*, 2004] because of unique tectonic forcing, including the huge thermal contrasts between the world's largest continent, Eurasia, and the largest ocean basin, the Pacific, and strong dynamic and thermodynamic influence of the world's highest land feature, the Tibetan Plateau. The EASM has characteristic features in both rainfall distribution and associated large-scale circulation systems [e.g., *Wang et al.*, 2008c].

[10] To quantitatively measure the strength of the EASM, a unified index, namely, the reversed *Wang and Fan* [1999] index (EASMI), is employed in this study. *Wang et al.* [2008c] compared 25 existing EASM indices and found this index has the best performance in capturing the total variance of the precipitation and three-dimensional circulation over east Asia, and it is nearly identical to the leading principal component of the EASM. The EASMI is defined by the $U850$ averaged in (22.5–32.5°N, 110–140°E) minus $U850$ in (5–15°N, 90–130°E) (red boxes in Figure 1), where $U850$ denotes the zonal wind at 850 hPa.

[11] Figure 1 presents JJA regressed precipitation to the EASMI. The rainfall distribution associated with the EASM shows a meridional tripole pattern with dry anomalies over the northern South China Sea (SCS) and Philippine Sea (the intertropical convergence zone or monsoon trough) and enhanced precipitation along the Yangtze River valley to southern Japan (the prevailing subtropical front) and over the Maritime Continent. Note that the EASMI highlights the significance of the Meiyu-Baiu-Changma rainfall in gauging the strength of the EASM because the Meiyu-Baiu-Changma rainfall, which is produced in the primary rain-bearing system, the east Asian subtropical front, better represents the variability of the EASM circulation system [*Wang et al.*, 2008c]. As such, the EASMI reverses the traditional Chinese meaning of a strong EASM which corresponds to a deficient Meiyu. The new definition is consistent with the meaning used in other monsoon regions worldwide where abundant rainfall within the major local

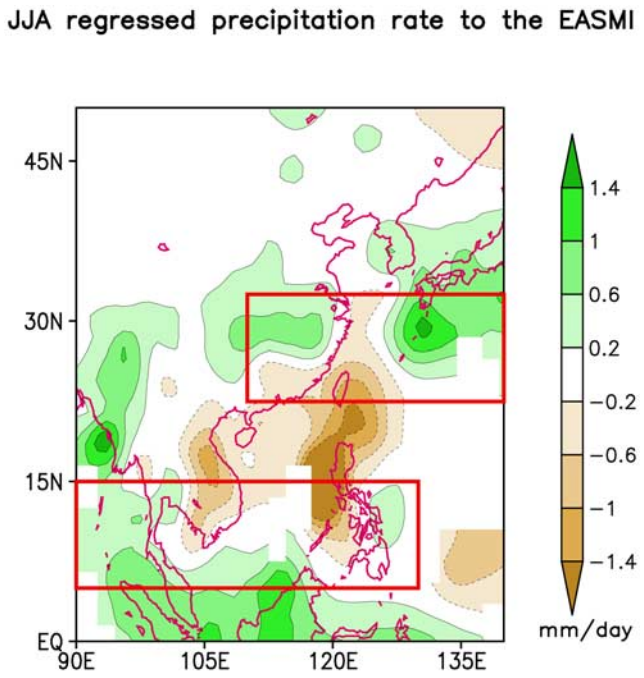

Figure 1. Anomalous summer (JJA) mean precipitation rate (color shading, see scale at right) that is regressed to the EASM index (EASMI). The precipitation data used are derived from PREC/L [*Chen et al.*, 2002] for the period of 1979–2006. The EASMI is an inverse Wang-Fan index [*Wang and Fan*, 1999; *Wang et al.*, 2008c] and is defined as the 850 hPa area-averaged zonal wind difference between the two red boxes (the north box minus the south box).

rain-bearing monsoon system is considered to be a strong monsoon [*Wang et al.*, 2008c].

[12] Figure 2 displays the anomalous global circulation structure accompanying a strong EASM. At 850 hPa, a prominent feature over east Asia is the anomalous subtropical high with enhanced southwesterly winds on its northwest flank prevailing from South China to the middle and lower reaches of the Yangtze River and southern Japan and strengthened easterly anomalies between 5° and 20°N (Figure 2a). A negative geopotential high anomaly belt controls the Meiyu-Baiu-Changma frontal area, which implies a strengthened east Asian subtropical front. A similar feature exists at 500 hPa over east Asia (Figure 2b), which is consistent with the suppressed rainfall anomaly over the northern SCS and Philippine Sea and abundant subtropical frontal rainfall (Figure 1). At 200 hPa, a large-scale anticyclone anomaly covers south China and expands eastward, and a cyclonic anomaly is over the Philippines and extending eastward (Figure 2c). The western Pacific subtropical high basically exhibits a baroclinic structure.

[13] It should be emphasized that in Figure 2, an Atlantic-Eurasian wave train of a barotropic structure controls the midlatitudes to high latitudes north of 50°N, extending from the North Atlantic to the Okhotsk Sea. Associated with this wave train pattern, three positive geopotential height anomaly centers are located at the North Atlantic, the Ural Mountains, and the Okhotsk Sea. Many previous studies already noticed that the blocking highs near the Ural Mountain and the Okhotsk Sea can have important effects on the EASM [e.g., *National Climate Center of China* (*NCC*), 1998; *Yang*, 2001; *Li and Ding*, 2004; *Ding and Sikka*, 2006]. This wave train pattern is different from the circumglobal teleconnection wave train pattern documented by *Ding and Wang* [2005]. The latter is associated with Indian summer monsoon. What triggers the Atlantic-Eurasian wave train? We will address this issue in section 5.

[14] On the basis of the above results, the EASM may be influenced not only by climate anomalies originated from the tropics but also by those from the midlatitudes to high latitudes in the Northern Hemisphere.

4. Spring NAO, North Atlantic SSTs, and EASM

[15] To further investigate the relationship between the EASM and spring NAO, we calculated correlation coefficients between the EASMI and the NAO index (NAOI) in

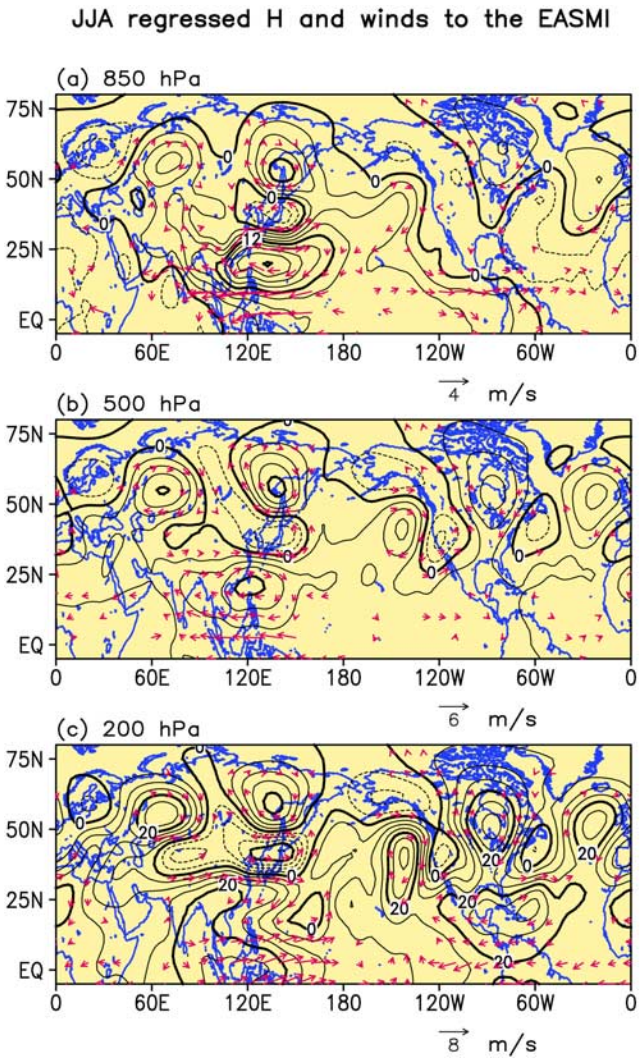

Figure 2. Anomalous summer (JJA) mean geopotential high (H) (contours in units of m), and winds (arrows, see scale at bottom right) that are regressed to the EASMI at (a) 850 hPa, (b) 500 hPa, and (c) 200 hPa, respectively. Only the winds significant at the 95% confidence level are plotted.

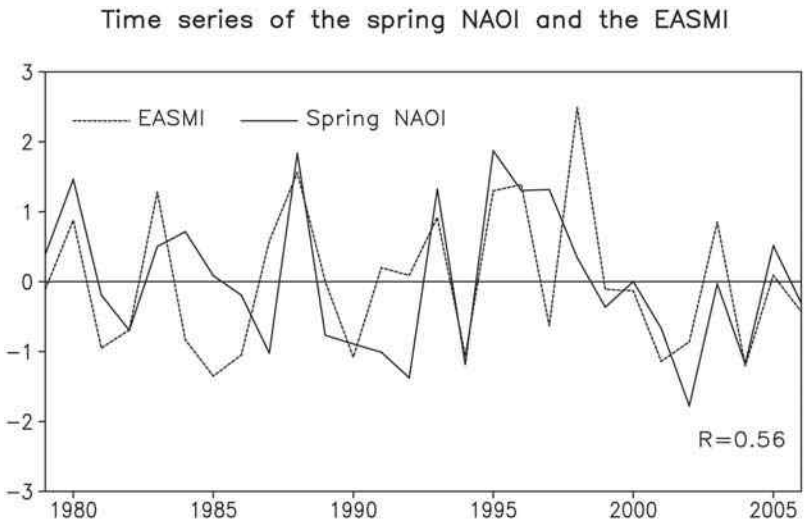

Figure 3. Time series of the EASMI and the spring (April–May) North Atlantic Oscillation (NAO) index (NAOI) [*Li and Wang*, 2003] for the 1979–2006 period. For convenience of comparison, the sign of NAOI is reversed. The correlation coefficient (R) between the EASMI and the spring NAOI is 0.56.

the six preceding months. The NAOI used in this study is defined as the difference in the normalized monthly sea level pressure (SLP) zonal-averaged over the North Atlantic sector from 80°W to 30°E between 35°N and 65°N [*Li and Wang*, 2003]. Through a systematic comparison of NAO indices, *Li and Wang* [2003] recommended that this NAOI provides a much more faithful and optimal representation of the spatial-temporal variability associated with the NAO, and it is also very simple.

[16] We found that the spring (April–May) NAOI has best correlation with the EASM. Figure 3 shows time series of the EASMI and the spring NAOI. The correlation coefficient reaches 0.56 for the period of 1979–2006, which is statistically significant at 99% confidence level based on a Student's *t* test. Note that for comparison, the sign of the spring NAOI in Figure 3 was reversed. The correlation coefficients between the two indices reach 0.7 and 0.52 on decadal trend and interannual time scales, respectively, all exceeding 95% confidence level. It indicates that the spring NAO is highly related to the EASM not only on a decadal trend time scale but also on an interannual time scale.

[17] Figure 4a displays the correlation pattern between the EASMI and spring SLP, which resembles a similar pattern with that between the spring NAOI and spring SLP (Figure 4b). Their pattern correlation coefficient reaches 0.81, beyond 99% confidence level. Significant negative correlation values are centered along the southeastern coast of North America, extending eastward, while significant positive values prevail in the high latitudes around Iceland. It suggests that anomalously weak spring NAO usually yields a precursory signal for a high EASMI summer and vice versa.

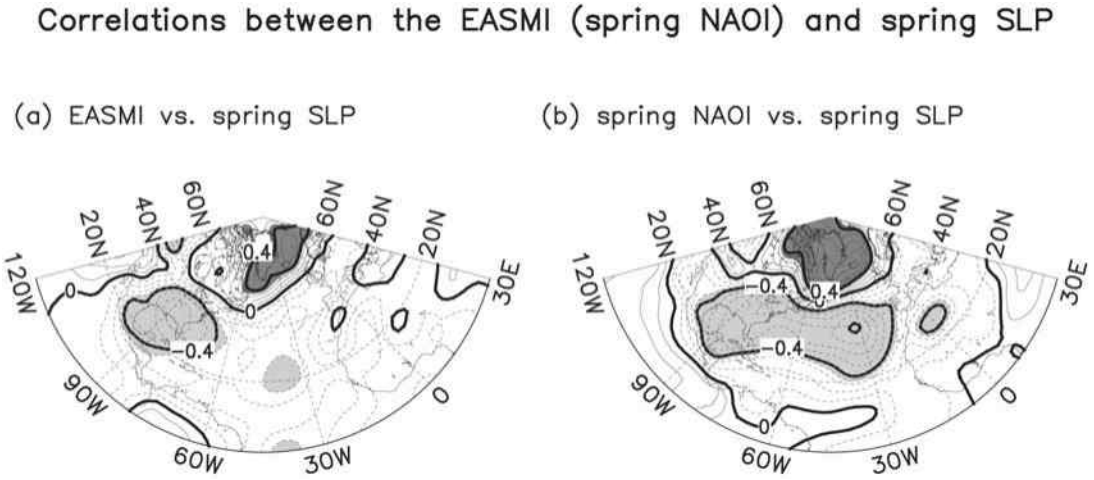

Figure 4. Correlation maps between sea level pressure (SLP) during the preceding spring (April–May) and (a) the JJA EASMI and (b) the spring NAOI. The dark (light) shading areas represent statistically significant positive (negative) correlation at 95% confidence interval.

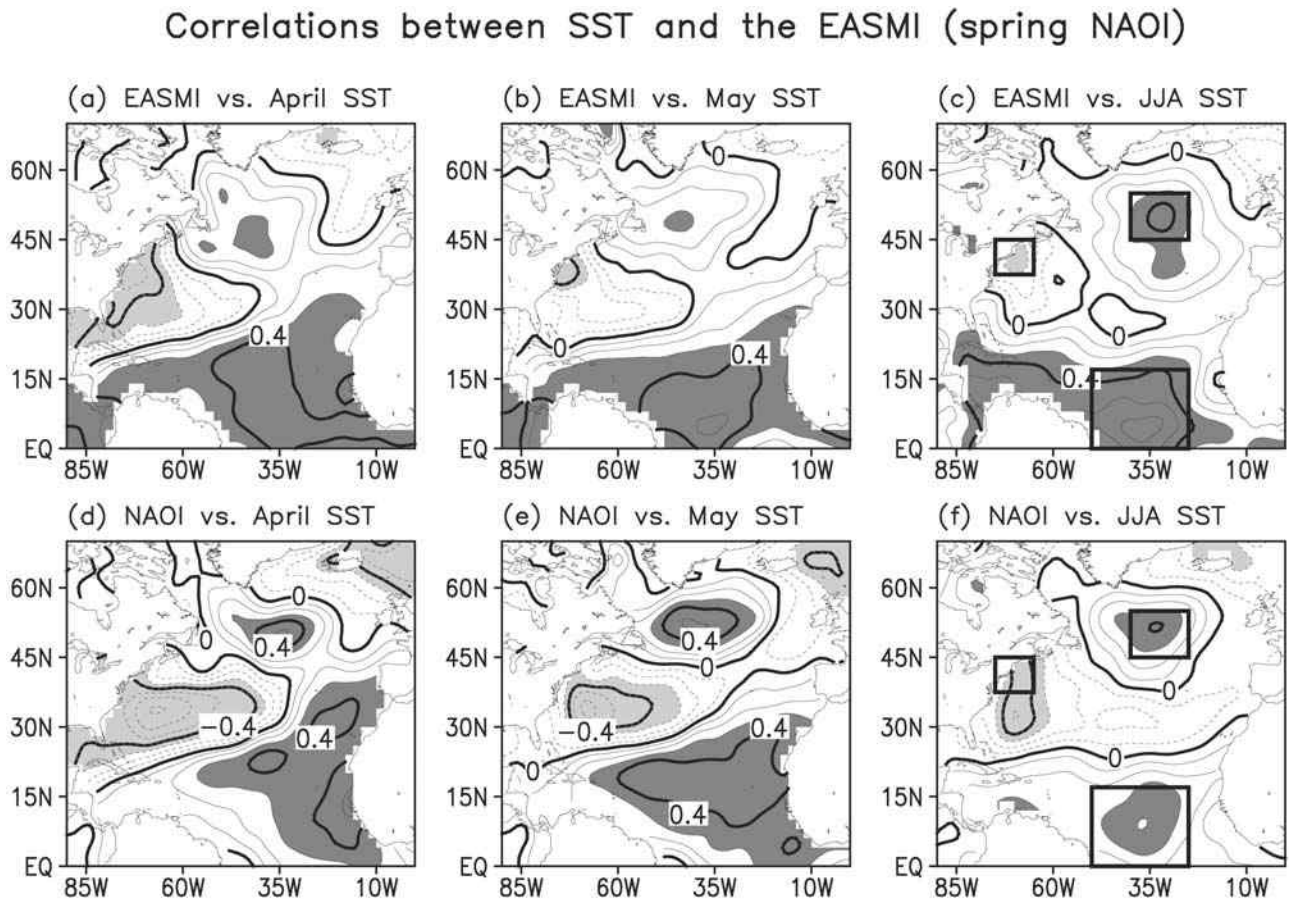

Figure 5. (a–c) Correlation maps between the JJA EASMI and North Atlantic sea surface temperature (SST) anomalies from the preceding April through the following JJA. The dark (light) shadings are significant positive (negative) correlation areas exceeding 95% confidence level. (d–f) The same as top except for the spring (April–May) NAOI. For comparison, the sign of NAOI is reversed.

[18] Since the atmosphere (or NAO), on its own, lacks the mechanisms to generate predictable variations, potential predictability of such fluctuations can only arise from coupled mechanisms that involve low boundary forcing such as SST [*Namias*, 1959, 1965; *Charney and Shukla*, 1981; *Shukla*, 1998]. Figure 5 shows SST correlation patterns with the EASMI and the spring NAOI from the preceding spring through the following summer. A pronounced feature is that the EASM and the spring NAO share a similar set of SST correlation patterns in the North Atlantic, i.e., a tripole pattern, which persists from the preceding spring through the following summer. *Watanabe et al.* [1999] and *Pan* [2005] found that such a North Atlantic tripole SST pattern is induced by anomalous NAO in boreal winter. According to the result in Figure 5, the tripole pattern is also likely to emerge in boreal spring if NAO anomalies occur. Furthermore, such a pattern is a relevant precursor for the EASM anomalies, which implies that it might contribute to the EASM variations. To quantitatively depict the tripole pattern during boreal summer, a simple tripole SST index (SSTI) is defined as the difference between the sum of averaged SST in two positive correlation boxes and averaged SST in the negative correlation box (positive domain minus negative domain). The tripole SSTI exhibits a nearly consistent variability with the EASMI, their correlation coefficient reaching 0.62 beyond 99% confidence level.

[19] From the above statistical analysis, the linkage among spring NAO, the North Atlantic SST anomalies, and the EASM may be summarized as the following: spring NAO anomalies are usually associated with a tripole SST anomaly pattern in the North Atlantic which can persist from spring through summer; the summer tripole SST anomalies are significantly correlated to the EASM variations. However, the correlations do not warrant any cause and effect.

5. Physical Mechanisms

[20] How can spring NAO affect the EASM? To figure out this question, first we need to understand why spring NAO can induce a tripole SST pattern in the North Atlantic. Then, it should be asked what is responsible for the persistence of the tripole SST pattern through summer, in light of the crucial "bridge" role the tripole pattern plays in the linkage between spring NAO and the EASM. The last and most important issue is how the tripole SST anomaly pattern in the North Atlantic exerts effects on the EASM.

[21] It is generally recognized that NAO is of a barotropical structure and a most distinguished feature associated

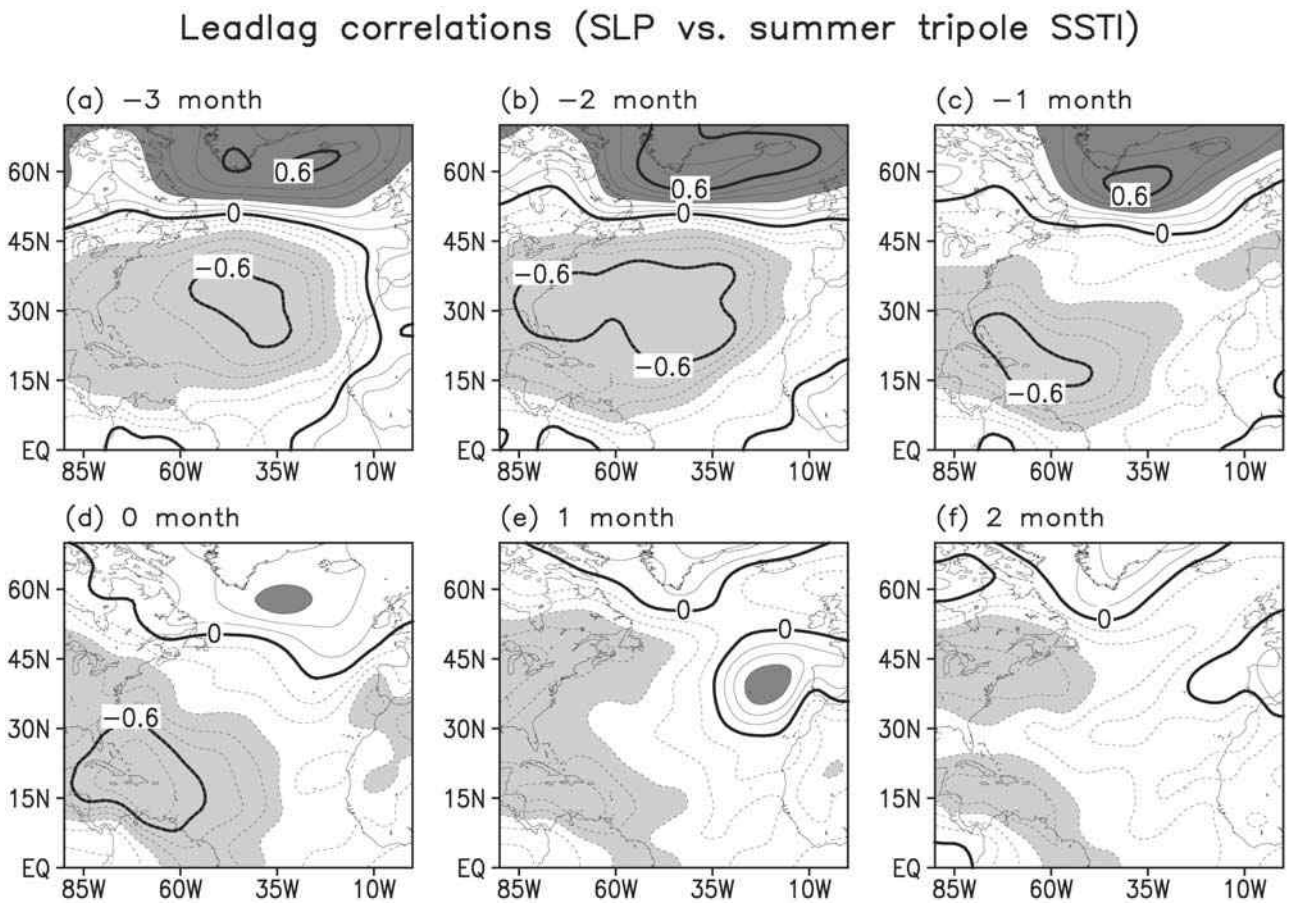

Figure 6. The lead-lag correlation patterns between the SLP and the summer tripole SSTI. The tripole SSTI leads the SLP by (a) −3, (b) −2, (c) −1, (d) 0, (e) 1, and (f) 2 months. The dark (light) shaded areas denote significant positive (negative) correlation exceeding 95% confidence level. Note that −3 months correspond to March–May, −2 months correspond to April–June, and so on.

with a strong (weak) NAO phase is the poleward (equatorward) displacement of the North Atlantic storm track [e.g., *Thompson and Wallace*, 2000a, 2000b; *Trenberth et al.*, 2005]. The surface wind speed varies in phase with the high-level jet stream (not shown); weak spring NAO phases are usually associated with high surface wind speed within (30–45°N) and low wind speed within the areas south of 30°N and north of 45°N and vice versa. For high (low) sea surface wind speed often favors cold (warm) SST anomalies by latent heat flux exchange, SST exhibits a similar pattern (positive correlations within poleward and equatorward areas and negative correlations in the middle latitudes) as a response to this tripole surface wind speed pattern. Therefore, the poleward (equatorward) displacement of the North Atlantic storm track associated with a strong (weak) NAO phase can account for the North Atlantic tripole SST pattern in spring just the same as it does in winter.

[22] Although previous studies found that positive feedbacks between NAO and tripole SST anomalies can sustain a tripole SST pattern in the North Atlantic during winter [*Watanabe et al.*, 1999; *Pan*, 2005], it is still not clear how the tripole SST pattern can persist from spring through summer. To investigate the relevant mechanism, we take the summer tripole SSTI as a reference and compute the lead-lag correlation with SLP fields. The results are shown in Figure 6. The absolute values of the correlation coefficients reach a maximum at a −2-month lead (Figure 6b), and then it continuously decreases from a 0-month lead (Figure 6d), to a 2-month lead (Figure 6f). The correlated SLP field from a −3-month through a −1-month lead (Figures 6a–6c) shows a NAO-like pattern [e.g., *Thompson and Wallace*, 2000a, 2000b; *Li and Wang*, 2003]. It indicates that NAO-like atmospheric anomalies are driving the ocean and producing a tripole-like SST anomaly pattern. This is similar to the results in winter [e.g., *Deser and Timlin*, 1997; *Pan*, 2005]. However, the NAO-like pattern weakens from a 0-month through a 2-month lead (Figures 6d–6f), illustrating that the tripole SST anomalies do not have a significant positive feedback to summer NAO-like atmosphere anomalies. This is different from the wintertime situation and has not been noticed before. It also implies that the persistence of the tripole SST pattern in summer may be due to the ocean memory effect.

[23] The assumption that the ocean memory effect plays a major role in the maintenance of the tripole SST pattern from spring to summer can be further confirmed by comparison of regressed SST patterns with reference to the summer tripole SSTI between the SST persistent component and the total SST. The persistent component of the SST,

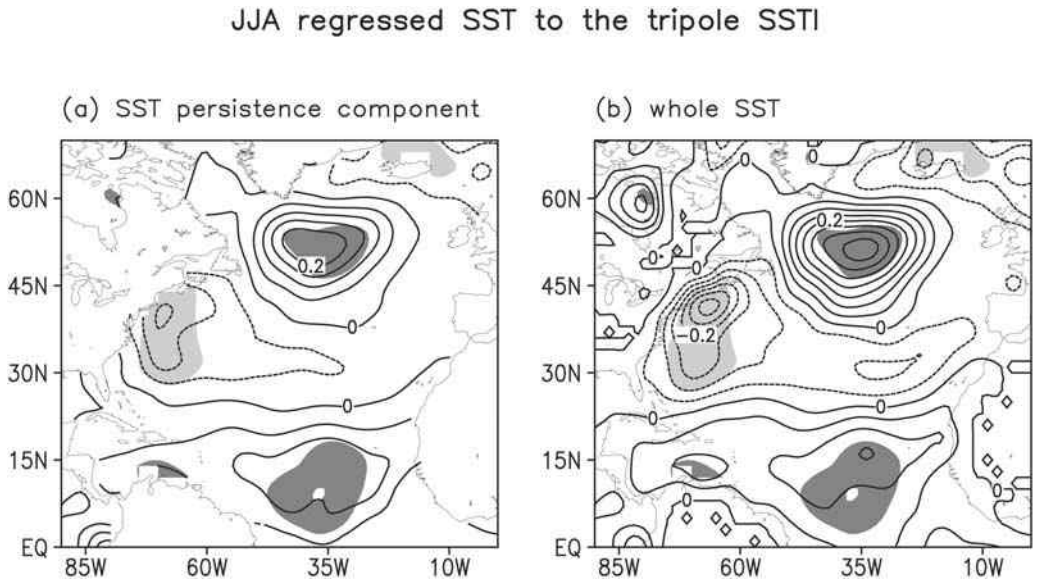

Figure 7. JJA mean SST anomaly patterns regressed to the tripole SSTI for (a) the persistence component of SST and (b) the total SST. The dark (light) shaded areas represent significant positive (negative) correlation exceeding 95% confidence level.

SST_p, at time $t + 1$ can be calculated according to the following formula [*Pan*, 2005]:

$$SST_p = SST(t)Cov[SST(t+1), SST(t)]/Var[SST(t)], \quad (1)$$

where $t + 1$ and t denote summer and spring, respectively. Cov and Var represent the covariance and variance, respectively. The regressed SST patterns with reference to the summer tripole SSTI for the SST persistent component and the total SST are shown in Figure 7. The dominant pattern of the SST persistent component (Figure 7a) does not change much compared to that of the total SST (Figure 7b), with the signal only decreasing slightly by about 10–20%. Thus, the ocean memory effect should be regarded as the crucial factor responsible for the persistence of the tripole SST anomaly pattern from spring to summer. This is different from the wintertime during which the positive feedbacks between the NAO and the underneath tripole SST anomalies are essential for sustaining the tripole SST pattern [e.g., *Pan*, 2005].

[24] To better understand large-scale circulation features coupled with the North Atlantic tripole SST anomalies during summer, Figure 8 presents JJA 200 hPa westerly

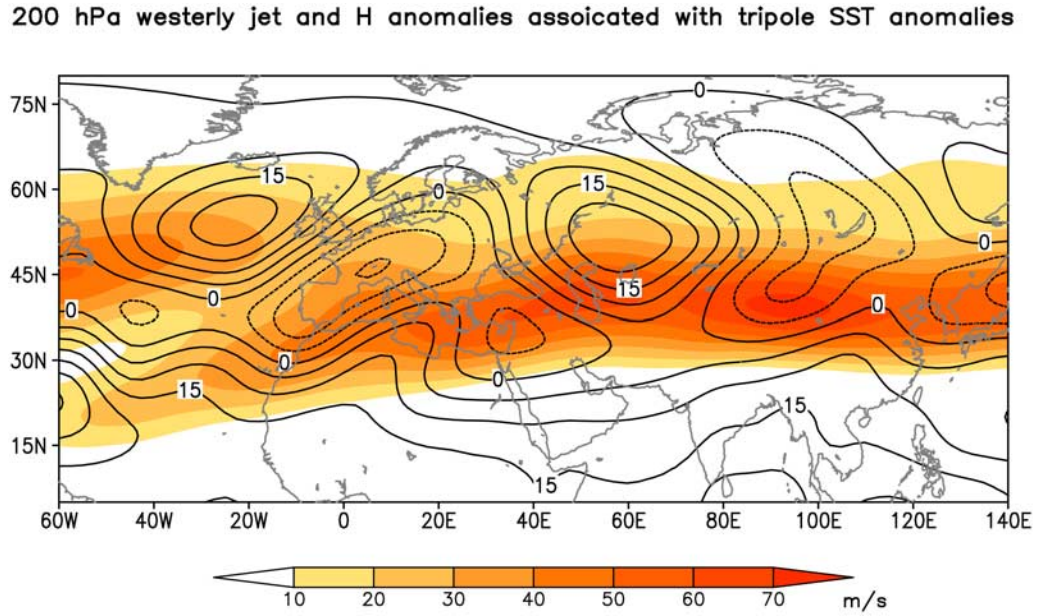

Figure 8. The 200 hPa westerly jet (color shadings in units of m/s) and H anomalies (contours in units of m) regressed to the tripole SSTI. The westerly jet is obtained through climatological JJA westerlies plus westerly anomalies regressed to the tripole SSTI.

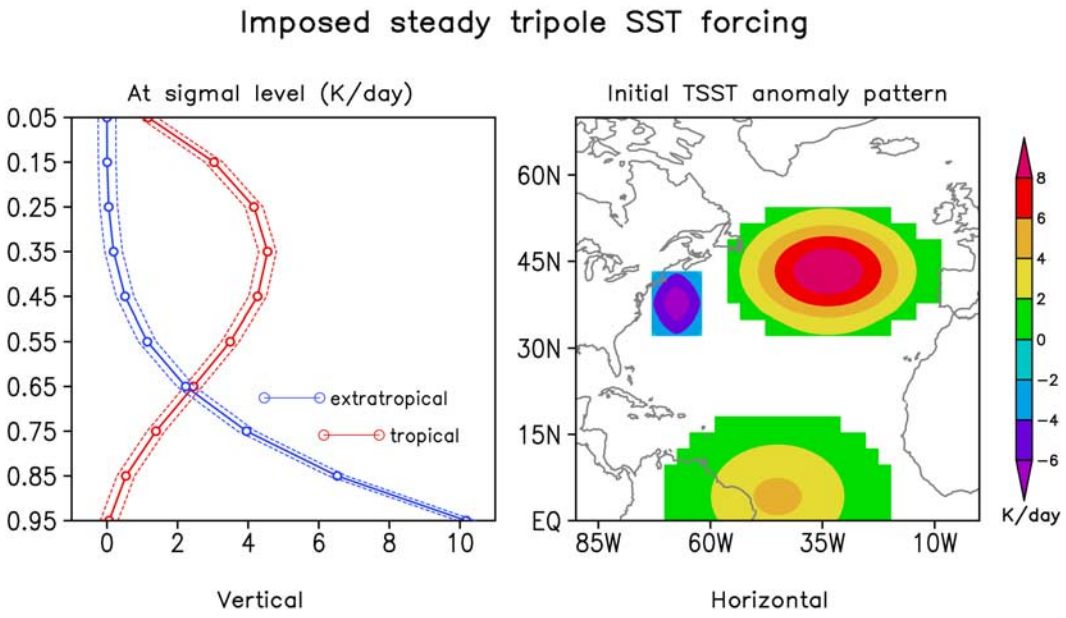

Figure 9. (left) Specified diabatic heating profiles (curves) and (right) SST anomaly pattern (color shadings) associated with a high tripole SSTI forcing in the numerical experiment with the SGCM. Note that the sign of a vertical profile is reversed for a negative SST anomaly. Maps for a low tripole SSTI forcing are mirror images of the plot shown here. TSST stands for the tripole SST.

jet (color shadings) associated with the tripole SST anomalies (the calculation method is shown in Figure 8) and geopotential high anomalies (contours) regressed to the tripole SSTI. A noticeable feature is that a systematic wave train pattern, characterized by three positive height anomalies over the North Atlantic, the Ural Mountain and the Okhotsk Sea, and two negative ones over western Europe and Mongolia, prevails along the poleward flank of the westerly jet. This feature is highly consistent with the wave train pattern associated the EASM discussed in section 3 (Figure 2c). Such a consistence allows us to interpret it as the impact of the anomalous tripole SST steady forcing on the EASM by inducing downstream development of subpolar teleconnections across the northern Eurasia.

[25] To further elucidate the effects of an anomalous North Atlantic tripole SST forcing on the EASM, we performed numerical experiments with the SGCM described in section 2. To mimic the diabatic heating effects of a high tripole SSTI forcing, we imposed two heating sources and one cooling source; each has an elliptical squared cosine distribution in latitude and longitude with a vertically integrated heating rate of 2.5 K/d (Figure 9, right). The vertical heating profile over the extratropical area is distinguished from that over the tropics as shown in Figure 9 (left) [*Hall et al.*, 2001a, 2001b; *Lin and Derome*, 1996]. Mimicking a low tripole SSTI forcing is the same as mimicking a high tripole SSTI forcing except for a reversed sign. To do the sensitivity study, we randomly changed the profile within the range between the two red (blue) dashed curves and did 10 integrations, with the average profile to be the same as the solid curves with empty circles (Figure 9, left). To make the numerical results more robust, the control run was integrated for 12 years and the last 10 years' integration was used to derive a reference state. The two sensitivity tests were integrated for 10 years each. The 10-year integrations were used to construct a 10-member ensemble (arithmetic) mean to reduce the uncertainties arising from differing initial conditions.

[26] Under the North Atlantic tripole SST anomaly forcing, the simulation basically captures the downstream development of subpolar teleconnections across northern Eurasia, with the pattern correlation coefficient between the observation and the simulation reaching 0.25 over the region north of 50°N and exceeding 99.9% confidence level (Figure 10). The downstream development of subpolar teleconnections across northern Eurasia raises (or lowers) the pressure over the Ural Mountain and the Okhotsk Sea. When the North Atlantic is in a high (low) tripole SSTI phase, the corresponding wave train across the northern Eurasia favors enhancement (weakening) of the blocking highs over the Ural Mountain and the Okhotsk Sea. As noted in many previous studies [e.g., *NCC*, 1998; *Yang*, 2001; *Li and Ding*, 2004; *Ding and Sikka*, 2006], the blocking highs near the Ural Mountain and the Okhotsk Sea usually facilitate a strengthened (weakened) east Asian subtropical front during summer, leading to a strong (weak) EASM. In such cases, the North Atlantic tripole SST anomalies are tied to the EASM variations. Note that the simulation has large discrepancies in the midlatitudes to low latitudes (south of 50°N), which implies that North Atlantic tripole SST anomalies cannot well interpret the circulation variations in the low latitudes and some other factors may dominate the low-latitude circulations. In fact, circulation variations over the east Asian low-latitude domain are more relevant to ENSO, as documented in details by *Wang et al.* [2008c]. It should be pointed out that we tried to add ENSO heating profiles to see whether the whole circulation can be realistically reproduced, but unfortunately this model has difficulty in depicting the prolonged influence of ENSO in the preceding winter (not shown). However, *Wang et al.*

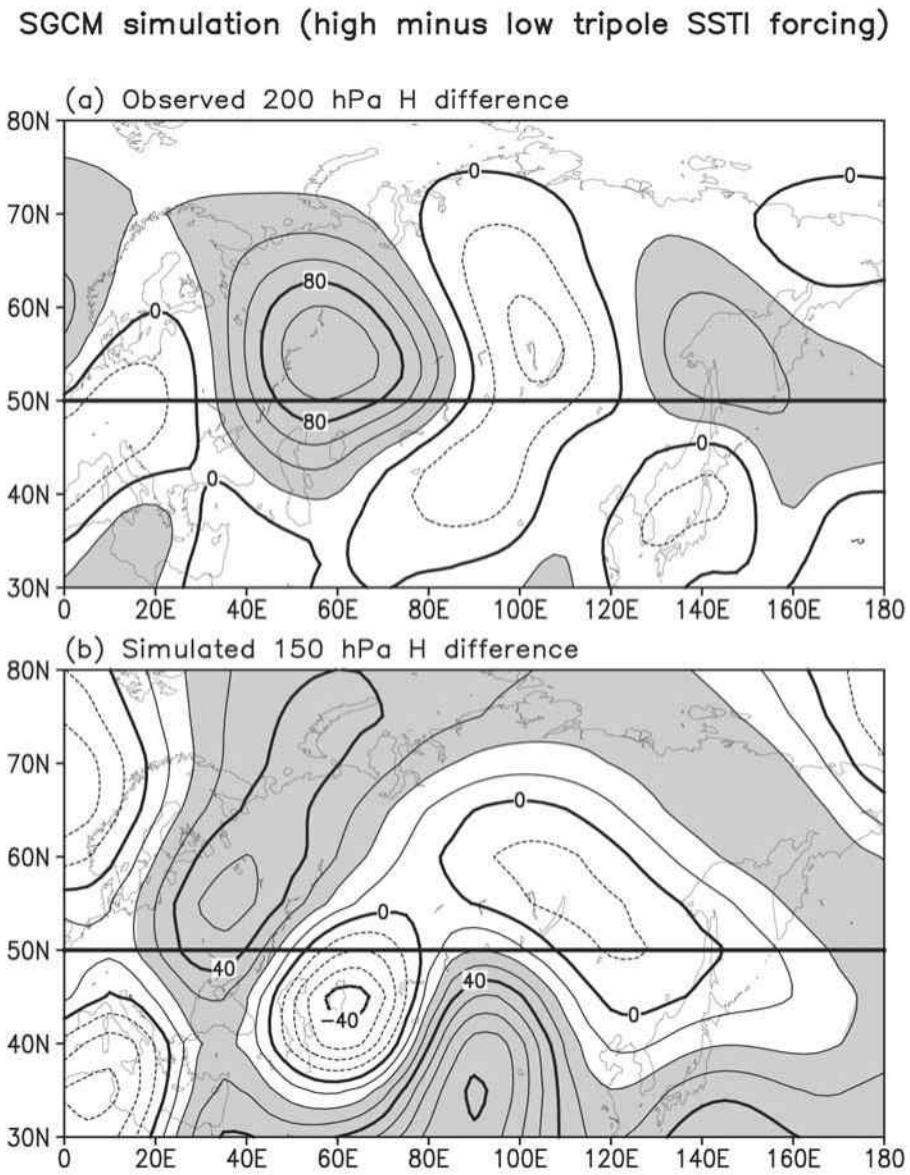

Figure 10. Comparison between the (a) observed 200 hPa H difference (contours in units of m) and the (b) simulated 150 hPa H difference (contours in units of m) regarding the high and low tripole SSTI forcing in summer (high minus low SSTI).

[2000] suggested that the interaction between the off-equatorial moist atmospheric Rossby waves and the underlying SST anomalies in the western Pacific warm pool region can "prolong" the impacts of ENSO from its mature phase to decaying phase and causes a "delayed" response of the EASM to ENSO. This mechanism is also further verified by the numerical experiments by *Lau and Nath* [2006]. Therefore, we do not focus too much on how the preceding ENSO can influence the EASM variations.

[27] To summarize, anomalous spring NAO can induce a tripole SST pattern in the North Atlantic which sustains from spring through summer. The summer tripole SST anomalies contribute to the downstream development of subpolar teleconnections across the northern Eurasia, which enhances (weakens) the high pressure over the Ural Mountain and the Okhotsk Sea. These favor a strengthened (weakened) east Asian subtropical front, namely, a strong (weak) EASM.

6. Seasonal Prediction

[28] It has been generally accepted that ENSO is the dominant predictor for the EASM [e.g., *Fu and Teng*, 1988; *Weng et al.*, 1999, *Wang et al.*, 2000, 2008c; *Chang et al.*, 2000a, 2000b; *Yang and Lau*, 2006]. ENSO affects the EASM not only on its decay phases but also on the development phases [*Wang et al.*, 2009]. The results in this study manifest that the spring NAO provides an additional physically based predictor for the EASM besides ENSO. To verify how well the spring NAO contributes to the prediction skill of the EASM, an empirical seasonal prediction model is developed using a linear regression

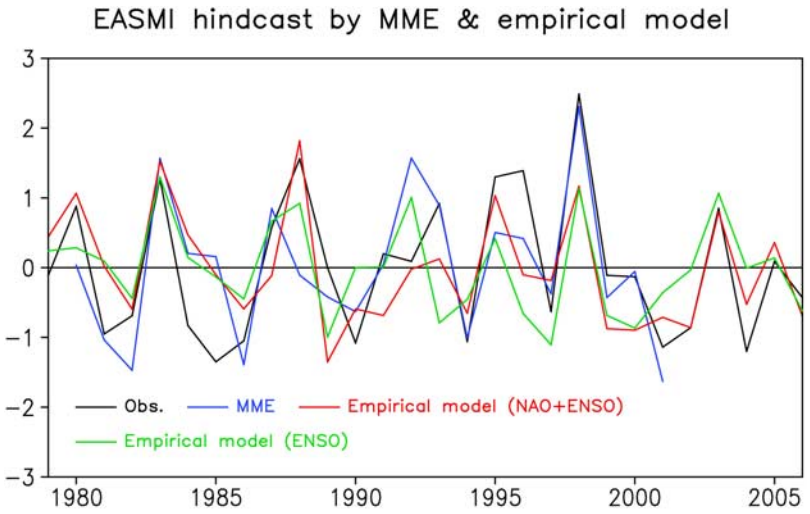

Figure 11. Comparison of the hindcast EASMI made by the empirical model (with and without NAO) and by the multimodel ensemble mean of the 14 state-of-the-art models.

method based on spring NAO and ENSO for the period of 1979–2006:

$$y = 7.52 + 0.65(\mathrm{NAOI}) + 0.25\left(\mathrm{ENSO}_{\mathrm{develop}}\right) - 0.3\left(\mathrm{ENSO}_{\mathrm{decay}}\right) \quad (2)$$

where NAOI and $\mathrm{ENSO}_{\mathrm{decay}}$ denote the NAO index value for April–May and Niño3.4 index for winter (December–February (DJF)), respectively. Here, we use $\mathrm{ENSO}_{\mathrm{develop}}$, the Niño3.4 index difference between April–May and February–March (the former minus the latter), and $\mathrm{ENSO}_{\mathrm{decay}}$, the Niño3.4 index in the preceding DJF to quantitatively measure the ENSO development and decay, respectively. The relative importance of the predictors to the overall model is ordered by $\mathrm{ENSO}_{\mathrm{develop}}$ (−0.62), $\mathrm{ENSO}_{\mathrm{decay}}$ (0.58), and NAOI (−0.56) in terms of the partial correlations in parentheses. The correlation between the simulation and the observation of the EASMI is 0.79.

[29] Note that we tried just using the change in the Niño3.4 index in (April–May) minus (February–March) (or March–May minus DJF, etc.) to quantify both ENSO decay and development, and the established empirical model had lower prediction skill than the current one. Although there is a significant correlation between the Niño3.4 index in December–February and the change in the index in (April–May) minus (February–March), they are not exactly same. Figure 3 of *Wang et al.* [2008c] may explain the reason. The Niño3.4 index in December–February has the highest correlation with the first leading mode of the EASM, but poorly correlated with the second mode, while the change in the Niño3.4 index in (April–May) minus (February–March) correlated well with both modes. Therefore, the change in the Niño3.4 index (April–May) minus (February–March) and the Niño3.4 index in DJF are complementary to each other. Nevertheless, there might be a better way to quantify the ENSO decay and development.

[30] To test the predictive capability of the empirical model, the cross-validation method [*Michaelsen*, 1987] is performed to hindcast the EASMI (1979–2006). To warrant the hindcast result robust, we choose a leaving-seven-out strategy [*Blockeel and Struyf*, 2002]. The relevant procedures are as follows: the cross-validation method systematically deletes 7 year from the period 1979–2006, derives a forecast model from the remaining years, and tests it on the deleted cases. Note that the choice of leaving seven out is not random. *Blockeel and Struyf* [2002] suggested that randomly choosing 20–30% of the data to be in a test data and the remainder as a training set for performing regression can prevent over fitting or wasting data. In our paper, 25% of the whole hindcast period (28 years) equals to 7 years. That is why we choose a leaving-seven-out strategy. The cross-validated estimates of the EASMI are shown in Figure 11. The correlation coefficient between the observation (black line in Figure 11) and the 28-year cross-validated estimates of the empirical model (red line in Figure 11) is 0.69. If we established the prediction model without the NAO included and did the same hindcast (green line in Figure 11), the correlation coefficient between the observation and the 28-year cross-validated estimates would be 0.5. It indicates that the NAO does significantly improve the seasonal prediction skill of the empirical model. For comparison, we also presented the observation and the MME hindcast (1980–2001) of the 14 state-of-the-art dynamic models participated in the Climate Prediction and Its Application to Society project. The hindcast of the new empirical model and that of the MME (blue line in Figure 11) are both in general agreement with the observation. The correlation coefficient between the observation and the 22-year MME hindcast is 0.74. The root-mean-square errors for the empirical model and the MME are 0.74 and 1.5, both comparable to the observed variance (being 1.0) and the empirical model better than the MME.

[31] It has been generally recognized that the MME is better than any single model prediction and increasing ensemble number of AGCMs can produce a better prediction skill [*Doblas-Reyes et al.*, 2000; *Palmer et al.*, 2000; *Krishnamurti et al.*, 1999]. Although the empirical model is very simple, it can generate a comparative skill with the 14 state-of-the-art dynamic models MME. Since the predictors

can be easily monitored in real time, this empirical model can be applied in practical forecast without relying on preforecasted SST.

7. Summary and Discussion

[32] The seasonal prediction of the EASM rainfall is of central importance, as it affects a quarter of world's population. The attempt to predict the east Asian monsoon variation started 75 years ago [e.g., *Zhu*, 1934; *Tu and Huang*, 1944], and it has become a focal issue in recent years [*Wang et al.*, 2004, 2005; *Wu and Li*, 2008]. Previous research works point out that the EASM variations are intimately linked to the development and decay of El Niño or La Niña [e.g., *Wang et al.*, 2008c, 2009]. Nevertheless, since the EASM encompasses tropics, subtropics, and midlatitudes, it is not only influenced by the climate and weather systems originated from the tropics but also those from midlatitudes to high latitudes [e.g., *Enomoto et al.*, 2003; *Wu et al.*, 2006; *He et al.*, 2006; *Ding and Wang*, 2007].

[33] This paper presents observed evidence and numerical experiment results to show that spring NAO can exert effects on the EASM, which has never been noticed before. Anomalous spring NAO can induce a tripole SST pattern in the North Atlantic which sustains from spring through summer. No significant feedbacks have been observed in summer between the tripole SST pattern and NAO-like atmosphere anomalies and the persistence of the tripole SST pattern is basically due to the ocean memory effect. Numerical experiments with the SGCM [e.g., *Hoskins and Simmons*, 1975; *Lin and Derome*, 1996] further reveal that the North Atlantic tripole SST anomalies in summer may contribute to the downstream development of subpolar teleconnections across the northern Eurasia, which enhances (weakens) the high over the Ural Mountain and the Okhotsk Sea. These favor a strengthened (weakened) east Asian subtropical front, resulting in a strong (weak) EASM. In such cases, variability of the spring NAO is tied to the EASM variability.

[34] The intimate linkage between spring NAO and the EASM provides another physical background to facilitate seasonal prediction of the EASM. On the basis of the above results, an empirical model is established to predict the EASM strength by the combination of ENSO and spring NAO. Hindcast is performed for the 1979–2006 period, which shows a comparative prediction skill with the MME hindcast of 14 start-of-the-art models. Since all these predictors are monitored in real time before the summer monsoon, this empirical model can be readily applied in practical forecast.

[35] How to quantify the ENSO impacts might need further investigations. In this study, we used the change in the Niño3.4 index in (April–May) minus (February–March) and the DJF Niño3.4 index to quantify ENSO development and decay, respectively. However, there might be a better way to quantify the ENSO phases. If so, the prediction skill of the empirical model might get even better.

[36] This seasonal prediction scenario is based on the seasonal mean time scale and the EASM dominant mode is assumed to be stable. However, many climate extreme events occur on a subseasonal time scale. Can this scenario predict the subseasonal events? If not, what are the sources of predictability for the subseasonal extreme events? Moreover, if the EASM leading mode changes over time, the predictors and relevant mechanisms may change, correspondingly. These are still open questions for future investigations.

[37] **Acknowledgments.** The authors thank the reviewers for helpful comments. The authors are also thankful for stimulating discussions with Tim Li, Shangping Xie, Pao-Shin Chu, and Q.-H. Ding. Bin Wang and Zhiwei Wu are supported by NSF climate dynamics program (ATM03–29531) and in part by IPRC, which is in part sponsored by FRCGC/JAMSTEC, NASA, and NOAA. Zhiwei Wu and Jianping Li acknowledge the support of the National Basic Research Program "973" (grant 2006CB403600) and the National Natural Science Foundation of China (grant 40605022).

References

Barnston, A. G., and R. E. Livezey (1987), Classification, seasonality and persistence of low-frequency atmospheric circulation patterns, *Mon. Weather Rev.*, *115*, 1083–1126, doi:10.1175/1520-0493(1987)115<1083:CSAPOL>2.0.CO;2.

Bjerknes, J. (1964), Atlantic air-sea interaction, *Adv. Geophys.*, *10*, 1–82.

Blockeel, H., and J. Struyf (2002), Efficient algorithms for decision tree cross- validation, *J. Mach. Learning Res.*, *3*, 621–650, doi:10.1162/jmlr.2003.3.4-5.621.

Chang, C.-P. (2004), Preface, in *East Asian Monsoon*, edited by C.-P. Chang, pp. v–vi, World Sci., Singapore.

Chang, C.-P., Y. Zhang, and T. Li (2000a), Interannual and interdecadal variation of the east Asian summer monsoon rainfall and tropical SSTs. Part 1: Roles of the subtropical ridge, *J. Clim.*, *13*, 4310–4325, doi:10.1175/1520-0442(2000)013<4310:IAIVOT>2.0.CO;2.

Chang, C.-P., Y. Zhang, and T. Li (2000b), Interannual and interdecadal variation of the east Asian summer monsoon rainfall and tropical SSTs. Part 2: Meridional structure of the monsoon, *J. Clim.*, *13*, 4326–4340, doi:10.1175/1520-0442(2000)013<4326:IAIVOT>2.0.CO;2.

Chang, C.-P., P. Harr, and J. Ju (2001), Possible roles of Atlantic circulations on the weakening Indian monsoon–ENSO relationship, *J. Clim.*, *14*, 2376–2380, doi:10.1175/1520-0442(2001)014<2376:PROACO>2.0.CO;2.

Charney, J. G., and J. Shukla (1981), Predictability of monsoons, in *Monsoon Dynamics*, edited by J. Lighthill and R. P. Pearce, pp. 99–109, Cambridge Univ. Press, New York.

Chen, G. T. J., and C.-P. Chang (1980), Structure and vorticity budget of early summer monsoon trough (Mei-yu) over southeastern China and Japan, *Mon. Weather Rev.*, *108*, 942–953, doi:10.1175/1520-0493(1980)108<0942:TSAVBO>2.0.CO;2.

Chen, M., P. Xie, J. E. Janowiak, and P. A. Arkin (2002), Global land precipitation: A 50-yr monthly analysis based on gauge observations, *J. Hydrometeorol.*, *3*, 249–266, doi:10.1175/1525-7541(2002)003<0249:GLPAYM>2.0.CO;2.

Deser, C., and M. Timlin (1997), Atmosphere-ocean interaction on weekly timescales in the North Atlantic and Pacific, *J. Clim.*, *10*, 393–408, doi:10.1175/1520-0442(1997)010<0393:AOIOWT>2.0.CO;2.

Ding, Y. H. (1992), Summer monsoon rainfalls in China, *J. Meteorol. Soc. Jpn.*, *70*, 397–421.

Ding, Y. H. (2004), Seasonal march of the east Asian summer monsoon, in *East Asian Monsoon*, edited by C.-P. Chang, pp. 3–53, World Sci., Singapore.

Ding, Y. H., and D. R. Sikka (2006), Synoptic systems and weather, in *The Asian Monsoon*, edited by B. Wang, pp. 131–201, Springer, New York.

Ding, Q., and B. Wang (2005), Circumglobal teleconnection in the Northern Hemisphere summer, *J. Clim.*, *18*, 3483–3505, doi:10.1175/JCLI3473.1.

Ding, Q., and B. Wang (2007), Intraseasonal teleconnection between the summer Eurasian wave train and the Indian monsoon, *J. Clim.*, *20*, 3751–3767, doi:10.1175/JCLI4221.1.

Doblas-Reyes, F. J., M. Deque, and J.-P. Piedelievre (2000), Multi-model spread and probabilistic seasonal forecasts in PROVOST, *Q. J. R. Meteorol. Soc.*, *126*, 2069–2088, doi:10.1256/smsqj.56704.

Enomoto, T., B. J. Hoskins, and Y. Matsuda (2003), The formation mechanism of the Bonin high in August, *Q. J. R. Meteorol. Soc.*, *129*, 157–178, doi:10.1256/qj.01.211.

Fu, C. B., and X. L. Teng (1988), Relationship between summer climate in China and El Niño/Southern Oscillation phenomenon (in Chinese), *Chin. J. Atmos. Sci.*, *12*, 133–141.

Gadgil, S., and S. Sajani (1998), Monsoon precipitation in the AMIP runs, *Clim. Dyn.*, *14*, 659–689, doi:10.1007/s003820050248.

Hall, N. M. J. (2000), A simple GCM based on dry dynamics and constant forcing, *J. Atmos. Sci.*, *57*, 1557–1572, doi:10.1175/1520-0469(2000)057<1557:ASGBOD>2.0.CO;2.

Hall, N. M. J., J. Derome, and H. Lin (2001a), The extratropical signal generated by a midlatitude SST anomaly. Part I: Sensitivity at equilibrium, *J. Clim.*, *14*, 2035–2053, doi:10.1175/1520-0442(2001)014<2035:TESGBA>2.0.CO;2.

Hall, N. M. J., J. Derome, and H. Lin (2001b), The extratropical signal generated by a midlatitude SST anomaly. Part II: Influence on seasonal forecasts, *J. Clim.*, *14*, 2696–2709, doi:10.1175/1520-0442(2001)014<2696:TESGBA>2.0.CO;2.

He, J. H., Z. W. Wu, Z. H. Jiang, C. S. Miao, and G. R. Han (2006), "Climate effect" of the northeast cold vortex and its influences on Meiyu, *Chin. Sci. Bull.*, *51*, 2803–2809.

Hoskins, B. J., and A. J. Simmons (1975), A multi-layer spectral model and the semi-implicit method, *Q. J. R. Meteorol. Soc.*, *101*, 637–655, doi:10.1002/qj.49710142918.

Huang, R. H., and L. Lu (1989), Numerical simulation of the relationship between the anomaly of subtropical high over east Asia and the convective activities in the western tropical Pacific, *Adv. Atmos. Sci.*, *6*, 202–214, doi:10.1007/BF02658016.

Jin, F.-F., L. Pan, and M. Watanabe (2006a), Dynamics of synoptic eddy and low-frequency flow interaction. Part 1: A linear closure, *J. Atmos. Sci.*, *63*, 1677–1694, doi:10.1175/JAS3715.1.

Jin, F.-F., L. Pan, and M. Watanabe (2006b), Dynamics of synoptic eddy and low-frequency flow interaction. Part 2: A theory for low-frequency modes, *J. Atmos. Sci.*, *63*, 1695–1708, doi:10.1175/JAS3716.1.

Kanamitsu, M., W. Ebisuzaki, J. Woollen, S.-K. Yang, J. J. Sling, M. Fiorino, and G. L. Potter (2002), NCEP-DOE AMIP-II reanalysis (R-2), *Bull. Am. Meteorol. Soc.*, *83*, 1631–1643, doi:10.1175/BAMS-83-11-1631(2002)083<1631:NAR>2.3.CO;2.

Kang, I.-S., et al. (2002), Intercomparison of the climatological variations of Asian summer monsoon precipitation simulated by 10 GCMs, *Clim. Dyn.*, *19*, 383–395, doi:10.1007/s00382-002-0245-9.

Krishnamurti, T. N., C. M. Kishtawal, T. E. LaRow, D. R. Bachiochi, Z. Zhang, C. E. Williford, S. Gadgil, and S. Surendran (1999), Improved weather and seasonal climate forecasts from multi-model superensemble, *Science*, *285*, 1548–1550, doi:10.1126/science.285.5433.1548.

Lau, N.-C., and M. J. Nath (1991), Variability of the baroclinic and barotropic transient eddy forcing associated with monthly changes in the midlatitude storm tracks, *J. Atmos. Sci.*, *48*, 2589–2613, doi:10.1175/1520-0469(1991)048<2589:VOTBAB>2.0.CO;2.

Lau, N.-C., and M. J. Nath (2006), ENSO modulation of the interannual and intraseasonal variability of the East Asian Monsoon—A model study, *J. Clim.*, *19*, 4508–4530, doi:10.1175/JCLI3878.1.

Lau, K.-M., G.-J. Yang, and S.-H. Shen (1988), Seasonal and intraseasonal climatology of summer monsoon rainfall over east Asia, *Mon. Weather Rev.*, *116*, 18–37, doi:10.1175/1520-0493(1988)116<0018:SAICOS>2.0.CO;2.

Li, F., and Y. H. Ding (2004), A statistical study of blocking highs in Eurasia in summer by using 30-yr NCEP datasets (in Chinese), *Acta Meteorol. Sin.*, *62*, 347–354.

Li, J., and J. Wang (2003), A new North Atlantic Oscillation index and its variability, *Adv. Atmos. Sci.*, *20*, 661–676, doi:10.1007/BF02690792.

Li, J., and Q. C. Zeng (2002), A unified monsoon index, *Geophys. Res. Lett.*, *29*(8), 1274, doi:10.1029/2001GL013874.

Lin, H., and J. Derome (1996), Changes in predictability associated with the PNA pattern, *Tellus, Ser. A*, *48*, 553–571.

Marshall, J. M., and F. Molteni (1993), Toward a dynamical understanding of planetary-scale flow regimes, *J. Atmos. Sci.*, *50*, 1792–1818, doi:10.1175/1520-0469(1993)050<1792:TADUOP>2.0.CO;2.

Michaelsen, J. (1987), Cross-validation in statistical climate forecast model, *J. Clim. Appl. Meteorol.*, *26*, 1589–1600, doi:10.1175/1520-0450(1987)026<1589:CVISCF>2.0.CO;2.

Namias, J. (1959), Recent seasonal interaction between North Pacific waters and the overlying atmospheric circulation, *J. Geophys. Res.*, *64*, 631–646, doi:10.1029/JZ064i006p00631.

Namias, J. (1965), Macroscopic association between monthly mean sea-surface temperature and overlying winds, *J. Geophys. Res.*, *70*, 2307–2318, doi:10.1029/JZ070i010p02307.

National Climate Center of China (NCC) (1998), *Heavy Flooding and Climate Anomalies in China in 1998*, 139 pp., Chin. Meteorol. Press, Beijing.

Ninomiya, K. (2004), Large- and mesoscale features of the Meiyu-baiu front associated with intense rainfalls, in *East Asian Monsoon*, edited by C.-P. Chang, pp. 404–435, World Sci., Singapore.

Palmer, T. N., C. Brankovic, and D. S. Richardson (2000), A probability and decision-model analysis of PROBOST seasonal multi-model ensemble integrations, *Q. J. R. Meteorol. Soc.*, *126*, 2013–2034, doi:10.1256/smsqj.56702.

Pan, L. (2005), Observed positive feedback between the NAO and the North Atlantic SSTA tripole, *Geophys. Res. Lett.*, *32*, L06707, doi:10.1029/2005GL022427.

Roads, J. O. (1987), Predictability in the extended range, *J. Atmos. Sci.*, *44*, 3495–3527, doi:10.1175/1520-0469(1987)044<3495:PITER>2.0.CO;2.

Shukla, J. (1998), Predictability in the midst of chaos: A scientific basis for climate forecasting, *Science*, *282*, 728–731, doi:10.1126/science.282.5389.728.

Simmons, A. J., and D. M. Burridge (1981), An energy and angular-momentum conserving vertical finite-difference scheme and hybrid vertical coordinates, *Mon. Weather Rev.*, *109*, 758–766, doi:10.1175/1520-0493(1981)109<0758:AEAAMC>2.0.CO;2.

Smith, T. M., and R. W. Reynolds (2004), Improved extended reconstruction of SST (1854–1997), *J. Clim.*, *17*, 2466–2477, doi:10.1175/1520-0442(2004)017<2466:IEROS>2.0.CO;2.

Sperber, K. R., and T. N. Palmer (1996), Interannual tropical rainfall variability in general circulation model simulations associated with the Atmospheric Model Intercomparison Project, *J. Clim.*, *9*, 2727–2750, doi:10.1175/1520-0442(1996)009<2727:ITRVIG>2.0.CO;2.

Tao, S., and L.-X. Chen (1987), A review of recent research on the east Asian summer monsoon in China, in *Monsoon Meteorology*, edited by C.-P. Chang and T. N. Krishnamurti, pp. 60–92, Oxford Univ. Press, New York.

Thompson, D. W. J., and J. M. Wallace (2000a), Annular modes in the extratropical circulation. Part I: Month-to-month variability, *J. Clim.*, *13*, 1000–1016, doi:10.1175/1520-0442(2000)013<1000:AMITEC>2.0.CO;2.

Thompson, D. W. J., and J. M. Wallace (2000b), Annular modes in the extratropical circulation. Part II: Trends, *J. Clim.*, *13*, 1018–1036, doi:10.1175/1520-0442(2000)013<1018:AMITEC>2.0.CO;2.

Trenberth, K. E., D. P. Stepaniak, and L. Smith (2005), Interannual variability of patterns of atmospheric mass distribution, *J. Clim.*, *18*, 2812–2825, doi:10.1175/JCLI3333.1.

Tu, C. W., and S. S. Huang (1944), The advance and withdrawal of Chinese summer monsoon (in Chinese), *Acta Meteorol. Sin.*, *18*, 1–20.

van Loon, H., and J. C. Rogers (1978), The seesaw in winter temperatures between Greenland and northern Europe. Part I: General description, *Mon. Weather Rev.*, *106*, 296–310, doi:10.1175/1520-0493(1978)106<0296:TSIWTB>2.0.CO;2.

Walker, G. T., and E. W. Bliss (1932), World weather V, *Mem. R. Meteorol. Soc.*, *4*, 53–84.

Wallace, J. M., and D. S. Gutzler (1981), Teleconnections in the geopotential height field during the Northern Hemisphere winter, *Mon. Weather Rev.*, *109*, 784–812, doi:10.1175/1520-0493(1981)109<0784:TITGHF>2.0.CO;2.

Wang, B., et al. (2008a), Advance and prospectus of seasonal prediction: Assessment of the APCC/CliPAS 14-model ensemble retroperspective seasonal prediction (1980–2004), *Clim. Dyn.*, *33*, 93–117, doi:10.1007/s00382-008-0460-0.

Wang, B., and Z. Fan (1999), Choice of South Asian summer monsoon indices, *Bull. Am. Meteorol. Soc.*, *80*, 629–638, doi:10.1175/1520-0477(1999)080<0629:COSASM>2.0.CO;2.

Wang, B., and T. Li (2004), East Asian monsoon and ENSO interaction, in *East Asian Monsoon*, edited by C.-P. Chang, pp. 172–212, World Sci., Singapore.

Wang, B., R. Wu, and X. Fu (2000), Pacific–east Asian teleconnection: How does ENSO affect east Asian climate?, *J. Clim.*, *13*, 1517–1536, doi:10.1175/1520-0442(2000)013<1517:PEATHD>2.0.CO;2.

Wang, B., R. Wu, and K.-M. Lau (2001), Interannual variability of Asian summer monsoon: Contrast between the Indian and western North Pacific–east Asian monsoons, *J. Clim.*, *14*, 4073–4090, doi:10.1175/1520-0442(2001)014<4073:IVOTAS>2.0.CO;2.

Wang, B., I.-S. Kang, and J.-Y. Lee (2004), Ensemble simulations of Asian-Australian monsoon variability by 11 AGCMs, *J. Clim.*, *17*, 803–818, doi:10.1175/1520-0442(2004)017<0803:ESOAMV>2.0.CO;2.

Wang, B., Q. Ding, X. Fu, I.-S. Kang, K. Jin, J. Shukla, and F. Doblas-Reyes (2005), Fundamental challenge in simulation and prediction of summer monsoon rainfall, *Geophys. Res. Lett.*, *32*, L15711, doi:10.1029/2005GL022734.

Wang, B., J.-Y. Lee, I.-S. Kang, J. Shukla, J.-S. Kug, A. Kumar, J. Schemm, J.-J. Luo, T. Yamagata, and C.-K. Park (2008b), How accurately do coupled climate models predict the Asian-Australian monsoon interannual variability?, *Clim. Dyn.*, *30*, 605–619, doi:10.1007/s00382-007-0310-5.

Wang, B., Z. Wu, J. Li, J. Liu, C.-P. Chang, Y. Ding, and G. Wu (2008c), How to measure the strength of the east Asian summer monsoon?, *J. Clim.*, *21*, 4449–4463, doi:10.1175/2008JCLI2183.1.

Wang, B., J. Liu, J. Yang, T. Zhou, and Z. Wu (2009), Distinct principal modes of early and late summer rainfall anomalies in east Asia, *J. Clim.*, *22*, 3864–3875, doi:10.1175/2009JCLI2850.1.

Watanabe, M. (2004), Asian jet waveguide and a downstream extension of the North Atlantic Oscillation, *J. Clim.*, *17*, 4674–4691, doi:10.1175/JCLI-3228.1.

Watanabe, M., M. Kimoto, and T. Nitta (1999), A comparison of decadal climate oscillations in the North Atlantic detected in observations and a coupled GCM, *J. Clim.*, *12*, 2920–2940, doi:10.1175/1520-0442(1999)012<2920:ACODCO>2.0.CO;2.

Weng, H.-Y., K.-M. Lau, and Y. Xue (1999), Multi-scale summer rainfall variability over China and its long-term link to global sea surface temperature variability, *J. Meteorol. Soc. Jpn.*, *77*, 845–857.

Wu, Z., and J. Li (2008), Prediction of the Asian-Australian monsoon interannual variations with the grid-point atmospheric model of IAP LASG (GAMIL), *Adv. Atmos. Sci.*, *25*, 387–394, doi:10.1007/s00376-008-0387-8.

Wu, G.-X., P. Liu, Y. Liu, and W. Li (2000), Impacts of sea surface temperature anomaly in the Indian Ocean on the subtropical cyclone over the western Pacific—Two-stage thermal adaptation in the atmosphere (in Chinese), *Acta Meteorol. Sin.*, *58*, 513–522.

Wu, Z. W., Z. H. Jiang, and J. H. He (2006), Comparison analysis of flood and drought features among the first flood period in south China, Meiyu period in the Yangtze River and Huaihe River valleys and rainy season in north China in the last 50 years (in Chinese), *J. Atmos. Sci.*, *30*, 391–401.

Yang, Y. W. (2001), The different effect of two types of blocking situation on major seasonal rain belt in China in July (in Chinese), *Acta Meteorol. Sin.*, *59*, 759–767.

Yang, S., and K.-M. Lau (2006), Interannual variability of the Asian monsoon, in *The Asian Monsoon*, edited by B. Wang, pp. 259–293, Springer, New York.

Zhu, K. Z. (1934), Southeastern monsoon and precipitation in China (in Chinese), *Acta Geogr. Sin.*, *1*, 1–27.

F.-F. Jin, Department of Meteorology, University of Hawai'i at Mānoa, 2525 Correa Road, Building HIG 350, Honolulu, HI 96822, USA.

J. Li and Z. Wu, State Key Laboratory of Numerical Modeling for Atmospheric Sciences and Geophysical Fluid Dynamics, Institute of Atmospheric Physics, Chinese Academy of Sciences, P.O. Box 9804, Beijing 100029, China.

B. Wang, IPRC, University of Hawai'i at Mānoa, 1680 East-West Road, POST Building 401, Honolulu, HI 96822, USA.